ACS APPLIED MATERIALS & INTERFACES

Research Article

www.acsami.org

Large Energy Storage Density and High Thermal Stability in a Highly Textured (111)-Oriented $Pb_{0.8}Ba_{0.2}ZrO_3$ Relaxor Thin Film with the Coexistence of Antiferroelectric and Ferroelectric Phases

Biaolin Peng,[†,‡,§] Qi Zhang,[∥,⊥] Xing Li,[§] Tieyu Sun,[§] Huiqing Fan,[#] Shanming Ke,[†] Mao Ye,[†,‡] Yu Wang,[§] Wei Lu,[§] Hanben Niu,[‡] Xierong Zeng,*[,†] and Haitao Huang*[,§]

[†]Shenzhen Key Laboratory of Special Functional Materials, Shenzhen Engineering Laboratory for Advanced Technology of Ceramics, College of Materials Science and Engineering, and [‡]Key Laboratory of Optoelectronic Devices and Systems of Ministry of Education and Guangdong Province, College of Optoelectronic Engineering, Shenzhen University, Shenzhen 518060, P. R. China

[§]Department of Applied Physics, The Hong Kong Polytechnic University, Kowloon, Hong Kong, China

[∥]Department of Manufacturing and Materials, Cranfield University, Cranfield, Bedfordshire MK43 0AL, United Kingdom

[⊥]State Key Laboratory of Advanced Technology for Materials Synthesis and Processing, Wuhan University of Technology, Wuhan 430070, Hubei, P. R. China

[#]State Key Laboratory of Solidification Processing, School of Materials Science and Engineering, Northwestern Polytechnical University, Xi'an 710072, China

ABSTRACT: A highly textured (111)-oriented $Pb_{0.8}Ba_{0.2}ZrO_3$ (PBZ) relaxor thin film with the coexistence of antiferroelectric (AFE) and ferroelectric (FE) phases was prepared on a $Pt/TiO_x/SiO_2/Si(100)$ substrate by using a sol–gel method. A large recoverable energy storage density of 40.18 J/cm^3 along with an efficiency of 64.1% was achieved at room temperature. Over a wide temperature range of 250 K (from room temperature to 523 K), the variation of the energy density is within 5%, indicating a high thermal stability. The high energy storage performance was endowed by a large dielectric breakdown strength, great relaxor dispersion, highly textured orientation, and the coexistence of FE and AFE phases. The PBZ thin film is believed to be an attractive material for applications in energy storage systems over a wide temperature range.

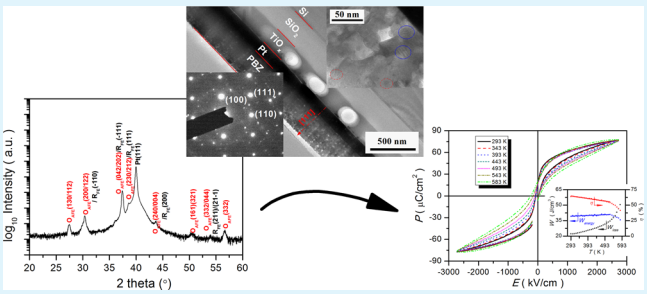

KEYWORDS: *energy storage, relaxor, antiferroelectric, textured, sol–gel*

1. INTRODUCTION

Recently, with the rapid development of microelectronic devices toward miniaturization, lightweightedness, and integration, new dielectric capacitors with higher energy storage density, fast charge/discharge, low cost, etc., are eagerly desired for applications in power electronics, pulsed power systems, etc.[1−5] Antiferroelectrics (AFEs) were predicted to be promising candidates for energy storage application as early as 1962.[2,6] However, for a long time, little attention was paid to them because of the low energy storage density in their bulk ceramics. For example, it was reported that the maximum energy storage density is only 2.75 J/cm^3 in conventional sintered ceramics[7−9] and only 3.2 J/cm^3 even in hot-pressed ceramics.[10]

It was recognized that the relatively low dielectric breakdown strength (normally less than 100 kV/cm) was one of the main reasons for the low energy density.[11−13]

With the development of modern thin-film technology such as sol–gel, pulsed-laser deposition, molecular beam epitaxy, etc., higher dielectric breakdown strength can be achieved in thin or thick films.[4,5,14,15] Thus, investigations on the energy storage properties of AFE films are receiving increasing attention. For instance, improved energy storage densities of about 14−18 J/cm^3 were obtained in Pr-, La-, Sr-, and Eu-doped $PbZrO_3$ thin films at room temperature.[16−19] Also, a large energy storage density of about 20.3 J/cm^3 at 6500 kV/cm was achieved in terpolymer nanocomposite thick films with 12 wt % boron nitride nanosheets.[20] Very recently, huge energy densities of 53 and 56 J/cm^3 at about 3500 kV/cm were reported in relaxor AFE $(Pb_{0.92}La_{0.08})(Zr_{0.9}Ti_{0.05})O_3$ and $(Pb_{0.97}La_{0.02})(Zr_{0.55}Sn_{0.4}Ti_{0.05})O_3$ thick films, respectively.[1,5] In addition to doping and composition optimization, many other efforts have been made to improve the energy storage density in AFE films, such as optimization of the grain size, phase purification, improvement in the crystallinity and orientation of thin films, etc.[7,14−16,21−23] However, in practical applications, a

Received: March 31, 2015
Accepted: May 21, 2015
Published: May 21, 2015

DOI: 10.1021/acsami.5b02790
ACS Appl. Mater. Interfaces 2015, 7, 13512−13517

competent energy storage material not only requires a high energy density but also a high thermal stability. So far, to the best of our knowledge, a large energy storage density with simultaneous high thermal stability in AFE films is rarely reported. Although large energy storage densities of 53 and 37 J/cm^3 have been achieved at 298 and 423 K, respectively, over a temperature range of ~130 K in AFE PLZT thin films,[5] the thermal stability is unacceptable for practical applications.

In this study, highly textured (111)-oriented $Pb_{0.8}Ba_{0.2}ZrO_3$ relaxor thin films with the coexistence of AFE and ferroelectric (FE) phases were fabricated by a sol–gel method. Large energy storage density (40.18 J/cm^3 at 2801 kV/cm) with high thermal stability (the variation of the energy density is within 5% from room temperature to 523 K) was achieved. Moreover, it is found that a highly textured structure can greatly improve the energy storage performance.

2. EXPERIMENTAL PROCEDURE

2.1. Fabrication of $Pb_{0.8}Ba_{0.2}ZrO_3$ (PBZ). A PBZ thin film was grown by using a sol–gel method. $Pb(OAc)_2{\cdot}3H_2O$ with 20% excess Pb and $Ba(CH_3COO)_2$ were dissolved in glacial acetic and deionized water. Simultaneously, appropriate acetylacetone was added to a mixture of 2-methoxyethanol and $Zr(O^nPr)_4$. The Pb/Ba and Zr solutions were then mixed and stirred for 2 h at room temperature. The final concentration of the PBZ precursor solution was 0.3 M. After aging of the precursor solution for 24 h, the PBZ thin film was deposited on $Pt(111)/TiO_x/SiO_2/Si(100)$ substrate through a multistep spin-coating technique. Each layer of the PBZ film was spin-coated at 4000 rpm for 30 s. To eliminate the formation of cracks, every wet film was first dried at 623 K for 3 min, subsequently pyrolyzed at 823 K for 3 min on hot plates, and finally crystallized at 1073 K for 3 min in a tube furnace in air. Layer by layer the spin coating and heat treatment were repeated several times to obtain the desired thickness. The final thickness of the PBZ thin film was about 320 nm, as determined by the cross-sectional micrographs.

2.2. Characterization. The crystallinity of the PBZ thin film was analyzed by X-ray diffraction (XRD; Rigaku 9 KW Smartlab, Tokyo, Japan). The cross-sectional morphology of the film was examined by scanning electron microscopy (FEI Sirion 200). The microstructure of the film was studied by transmission electron microscopy (TEM; JEOL JEM-2100F). The out-of-plane feature of the film was investigated by scanning probe microscopy (Bruker Multimode 8). The Raman scattering spectra were acquired by a Raman spectrometer (Horiba HR800) with an excitation laser wavelength of 488 nm. For measurement of the electrical properties, Au/Cr layers of 150 μm diameter were evaporated on the surface through a patterned photoresist mask to form a sandwiched electrode structure. Dielectric permittivity measurement was carried out using an impedance analyzer (Wayne-Kerr Electronics, West Sussex, U.K.) with a perturbation voltage V_{ac} = 100 mV. Polarization–electric field (P–E) hysteresis loops and current–voltage (I–V) curves were obtained by means of a ferroelectric tester (Precision Premier II, Radiant Technologies Inc., Alpharetta, GA) at 10 kHz. The energy storage performance was calculated according to the P–E loops.

3. RESULTS AND DISCUSSION

3.1. Structure. Figure 1 shows the XRD pattern of the PBZ thin film prepared by using a layer-by-layer crystallization process. The thin film exhibits good crystallinity and a pure perovskite phase with (111) preferential orientation. A possible reason for the (111) preferred growth of PBZ thin films on the Pt bottom electrode is that a thin layer of Pt_3Ti intermediates is formed during ceramic film crystallization, which favors formation of the (111) texture.[24] In addition to the rhombohedral FE phase, superlattice reflections with indices (130)/(112), (161)/(321), and (332) were also identified in

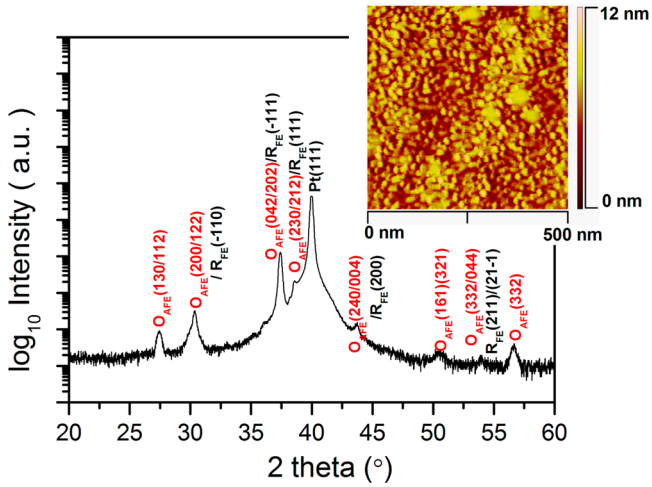

Figure 1. XRD pattern of the highly textured (111)-oriented PBZ thin film. Inset: AFM micrograph.

the PBZ thin film, indicative of the orthorhombic AFE phase.[25] A atomic force microscopy (AFM) micrograph (inset of Figure 1) reveals that the thin film has a low surface roughness, and the average R_a and R_q are 1.62 and 1.3 nm, respectively.[26]

Figure 2 shows the cross-sectional TEM image of the (111)-oriented PBZ thin film. It can be found that the PBZ thin film is

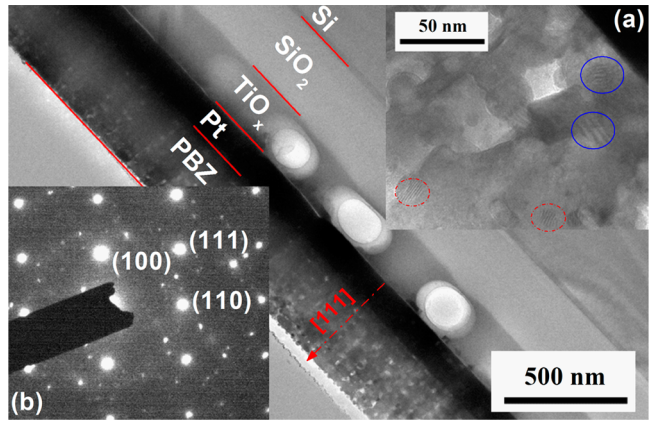

Figure 2. Cross-sectional TEM image of the highly textured (111)-oriented PBZ thin film. Insets: (a) an enlarged image of the thin film; (b) corresponding SAED pattern.

uniform, homogeneous, and crack-free, with a thickness of 320 nm. Nanocrystals with an average grain size of 20 nm in a highly ordered columnar-like texture is clearly visible in an enlarged image of the thin film (inset a of Figure 2). Inside some of the nanocrystals, lamellar nanodomains with ~1 nm width (the red dotted circles) and ~2 nm width (the blue solid circles) can be observed. The corresponding selected-area electron diffraction (SAED) pattern, which is labeled by using the pseudo cubic structure rather than the orthorhombic or rhombohedral one, indicates that the columnar-like texture is (111)-oriented, as shown in inset b of Figure 2.

3.2. Phase Transition. In order to understand the structure change of the highly textured (111)-oriented PBZ thin film, the Raman scattering spectrum was measured from 100 to 900 cm^{-1} in a temperature range between 298 and 463 K, in a step of 5 K. Representative plots of them are shown in Figure 3. Previous research work suggests that the appearance and

DOI: 10.1021/acsami.5b02790
ACS Appl. Mater. Interfaces 2015, 7, 13512–13517

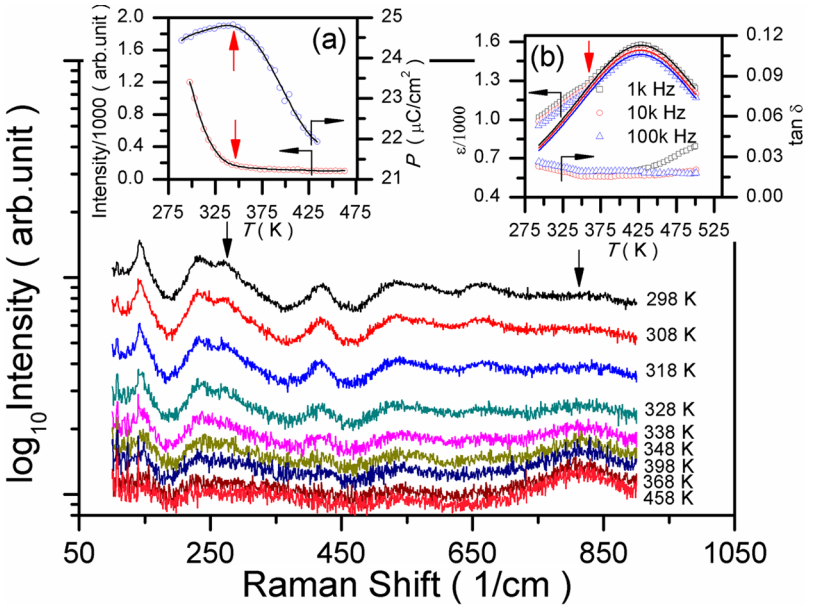

Figure 3. Raman scattering spectra of the highly textured (111)-oriented PBZ thin film. Insets: (a) temperature dependences of the Zr−O−Zr bending mode and the P_{max} measured at 156 kV/cm; (b) $\varepsilon(T)$ and tan $\delta(T)$.

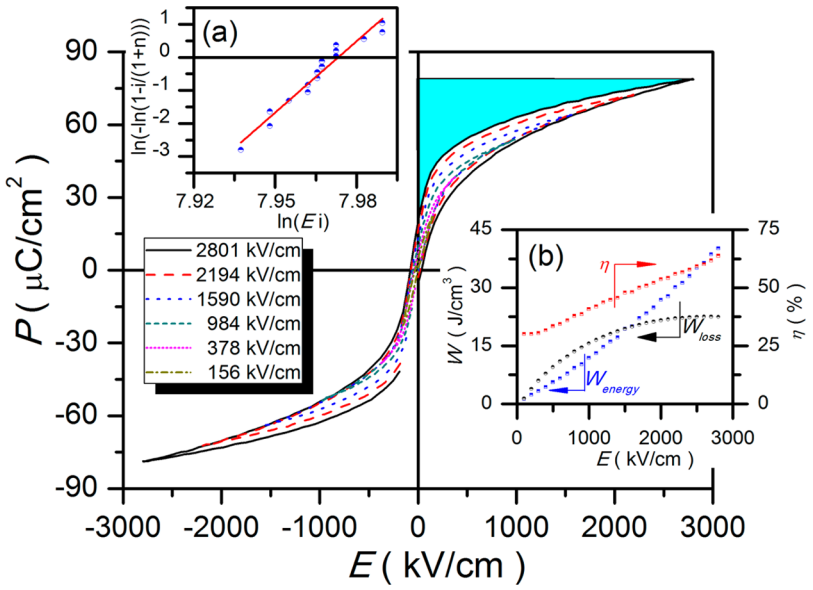

Figure 4. P−E loops of the highly textured (111)-oriented PBZ thin film at selected applied electric fields. The shaded area represents 40.18 J/m^3 being stored. Insets: (a) Weibull distribution for the dielectric breakdown strength; (b) W_{energy}, W_{loss}, and η versus E.

change of the band at 277 cm^{-1}, which is assigned to the Zr−O−Zr bending mode, can reflect the existence and change of the AFE phase in the $PbZrO_3$ thin film.[27] An additional active band at about 830 cm^{-1} is considered to be related to the appearance of the FE phase in a 3% W-doped $PbZrO_3$ thin film.[27,28] For the highly textured (111)-oriented PBZ thin film, the Zr−O−Zr bending mode exhibits a slight shift compared with the standard peak position (277 cm^{-1}) because of internal stress in the film.[23] The inset a of Figure 3 shows the temperature dependence of the Zr−O−Zr bending mode. It can be seen that the scattering intensity of the Zr−O−Zr bending mode degraded gradually with an increase of the temperature and disappeared at about 345 K, indicating completion of the AFE to FE phase transition. Meanwhile, a wide band around 830 cm^{-1} is found to become more and more significant with an increase of the temperature, which further confirms the existence of the AFE−FE phase transition.[23] Completion of the AFE−FE phase transition corresponds to the maximum polarization on the P−T curve, where P is obtained from the P−E loops measured at 156 kV/cm, as shown in inset a of Figure 3. The more subtle AFE−FE phase transition process can be detected by the temperature dependence of the dielectric permittivity and dielectric loss of the highly textured (111)-oriented PBZ thin film, as shown by the red arrow in inset b of Figure 3. The colored solid lines around the dielectric peak exhibit the best fitting result of the Lorentz-type relation $\varepsilon_A/\varepsilon = 1 + (T - T_A)^2/2\delta_A^2$.[29,30] A large δ_A (97.73) at 10 kHz is obtained and is close to that (103.6) of the prototypical relaxor $Pb(Mg_{1/3}Nb_{2/3})O_3$ ceramics, indicating a high degree of relaxor dispersion in the thin film. The

DOI: 10.1021/acsami.5b02790
ACS Appl. Mater. Interfaces 2015, 7, 13512−13517

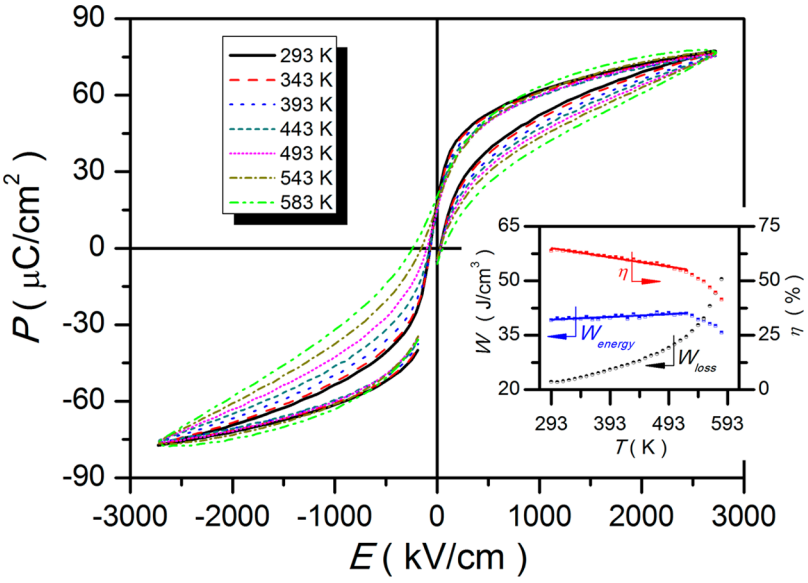

Figure 5. P–E loops of the highly textured (111)-oriented PBZ thin film at selected temperatures. Inset: W_{energy}, W_{loss}, and η versus T.

extrapolated dielectric permittivity on the low-temperature side of the dielectric peak gradually deviates from its measured value with decreasing temperature because of the coexistence of AFE and FE phases in the PBZ thin film.

3.3. Energy Storage. The recoverable energy density (W_{energy}) of a dielectric-based compound could be estimated from the P–E loops and calculated with the equation

$$W_{energy} = \int_{P_r}^{P_{max}} E \, dP, \qquad 0 \le E \le E_{max} \tag{1}$$

where E is the applied electric field that causes variation in the electric polarization P, P_r is the remnant polarization, and P_{max} is the maximum polarization under the applied field.[1−5] According to eq 1, materials simultaneously possessing smaller P_r, larger P_{max}, and higher breakdown strength are more favorable for energy storage. The above conditions are realized in the highly textured (111)-oriented PBZ relaxor film through the coexistence of FE and AFE phases, where the FE phase helps to maintain a high P_{max}, the AFE phase keeps a low P_r, and the relaxor characteristics release the large phase transition stress.[31]

Figure 4 shows the P–E loops of the highly textured PBZ thin film at selected applied electric fields. It can be seen that the P–E loop transforms gradually from a slim double loop into a single loop when the applied electric field is increased from 156 to 2801 kV/cm, indicating a field-induced AFE-to-FE phase transition. The maximum polarization P_{max} and the remnant polarization P_r at 2801 kV/cm are 19.76 and 78.68 μC/cm^2, respectively. Through integration of the discharging portion of the P–E loop according to eq 1, an energy density (W_{energy}) of 40.18 J/cm^3 (as painted by the cyan shaded area) at 2801 kV/cm can be achieved on the highly textured (111)-oriented PBZ thin film.

For energy storage applications, good electric field endurance is one of the crucial factors to consider. Inset a in Figure 4 depicts the Weibull distribution of the electric field breakdown strength (BDS) for the highly textured PBZ thin film. The values of BDS can be described by[32,33]

$$X_i = \ln(E_i) \tag{2}$$

$$Y_i = \ln\{\ln[1/(1 - P_i)]\} \tag{3}$$

$$P_i = i/(n + 1) \tag{4}$$

where n is the total number of samples, E_i is the breakdown electric field of the ith specimen arranged in ascending order ($E_1 \le E_2 \le E_3 ... \le E_n$), and P_i is the probability of dielectric breakdown. According to the two-parameter Weibull distribution, X_i and Y_i should have a linear relationship. The mean BDS can be extracted from the point where the fitting line intersects with the horizontal axis at $Y_i = 0$. According to the Weibull analysis, a statistical breakdown strength of 2902 kV/cm can be obtained. The high breakdown strength of the samples is attributed to their dense microstructure.

In practical applications, apart from the high recoverable energy density W_{energy}, large energy storage efficiency (η) is also desired, which is defined as the ratio of the discharging (output) energy to the charging (input) energy

$$\eta = W/(W + W_{loss}) \tag{5}$$

where W_{loss} is the energy loss density, calculated by the numerical integration of the closed area of the P–E hysteresis loops.[1−5] Inset b in Figure 4 depicts the electric field dependence of the energy density W_{energy}, the energy loss density W_{loss}, and the energy storage efficiency η. It can be seen that W_{energy} increases gradually with an increase of the applied electric field and reaches about 40.18 J/cm^3 at 2801 kV/cm. However, W_{loss} increases at small fields and then tends to be saturated at about 22.5 J/cm^3 at 2801 kV/cm. Similar to the trend of W_{energy}, the energy storage efficiency η increases with an increase of the applied electric field and reaches 64.1% at 2801 kV/cm. If a larger breakdown strength could be achieved for the highly textured PBZ thin film, based on the above results, a larger η and a constant W_{loss} could be inferred. Further enhancement in η can be achieved by appropriate doping of La to increase the degree of relaxor dispersion and maintain the AFE property. Moreover, η can also be enhanced by using oxide electrodes such as $LaNiO_3$.[14]

In addition to that above, the thermal stability of the energy storage performance should also be considered for real capacitor applications. Figure 5 shows P–E loops of the highly

DOI: 10.1021/acsami.5b02790
ACS Appl. Mater. Interfaces 2015, 7, 13512−13517

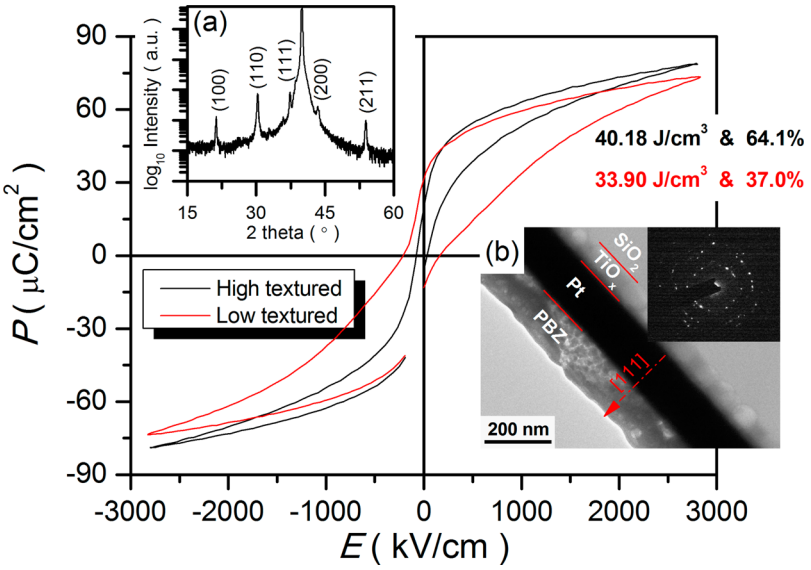

Figure 6. *P*–*E* loops of highly textured and less textured PBZ thin films. Insets: (a) XRD pattern; (b) cross-sectional TEM image and the corresponding SAED of a less textured PBZ thin film.

textured PBZ thin film in a wide temperature range of 293–583 K, which is measured at 2726 kV/cm, slightly lower than 2801 kV/cm to prevent the film from being thermally broken down. Inset a of Figure 5 summarizes the temperature dependence of W_{energy}, W_{loss}, and η. Clearly, W_{energy} increases slightly from room temperature (39.17 J/cm^3) up to 523 K (40.98 J/cm^3) and then decreases sharply. The variation of W_{energy} from room temperature to 523 K is within 5% (as shown by the blue solid line), indicating good thermal stability of the energy storage performance. The good thermal stability may be ascribed to the great relaxor dispersion of the highly textured PBZ thin film, as shown in inset b of Figure 3. Different from the behavior of W_{energy}, η decreases slowly from room temperature (63.84%) up to 523 K (54.26%) and then drops sharply. The variation of η in the above wide temperature range is within 15%. The sharp decreases of W_{energy} and η at above 523 K may be attributed to the reduction in the polarization and the increase in the leakage current (as reflected by the rounded ends of the green *P*–*E* loop in Figure 5)

To gain insight into the effect of texture on the energy storage performance of the highly textured (111)-oriented PBZ thin film, a less textured PBZ thin film was fabricated by a different deposition process. Instead of the layer-by-layer crystallization of the highly textured PBZ thin film, for the less textured PBZ thin film, each layer was dried at 623 K for 3 min and then pyrolized at 823 K for 5 min, after which the film was crystallized at 1023 K for 30 min in air. As shown by inset a of Figure 6, in addition to the (111) diffraction peak (for convenience, the lattice indices are labeled as a pseudocubic structure), very strong (110) and (100) diffraction peaks can also be detected in the XRD pattern, indicating a less textured film structure. The less textured film structure can also be confirmed by its cross-sectional TEM image and the corresponding SAED (inset b of Figure 6), where no obvious texture features can be detected.

Figure 6 shows the *P*–*E* loops of the highly textured and less textured PBZ thin films. A lower P_{max} (73.42 μC/cm^2) and a higher P_r (31.7 μC/cm^2), as well as a greater coercive field E_c (167 kV/cm), were obtained for the less textured PBZ thin film. W_{energy} and η of the less textured PBZ thin film are 33.9 J/cm^3 and 37%, respectively. Compared with those of the less textured PBZ thin film, W_{energy} (40.18 J/cm^3) in the highly textured PBZ thin film is increased by 18.5% and η (64.1%) is remarkably increased by 73.2%. These results indicate that the highly textured structure can help to improve the energy storage performance, especially for the energy efficiency η. Therefore, a larger W_{energy} and a higher η can be achieved in a highly (111)-oriented PBZ thin film.

4. CONCLUSIONS

A large recoverable energy storage density of 40.18 J/cm^3 and a high thermal stability (the variation of the energy storage density is within 5% from room temperature to 523 K) were simultaneously achieved in the highly textured (111)-oriented PBZ relaxor thin film with the coexistence of AFE and FE phases. This is accomplished by the large dielectric breakdown strength, great relaxor dispersion, high texture orientation, and coexistence of the FE and AFE phases. The excellent energy storage performance of the thin film may make it a promising material for applications in energy storage devices in a wide temperature range.

AUTHOR INFORMATION

Corresponding Authors

*E-mail: zengxier@szu.edu.cn.
*E-mail: aphhuang@polyu.edu.hk.

Notes

The authors declare no competing financial interest.

ACKNOWLEDGMENTS

This work was supported by the Hong Kong Polytechnic University (Projects A-PL54 and 1-ZVCG), the National Natural Science Foundation of China (Grants 51402196, 51272161, 51172187, and 51202150), the China Postdoctoral Science Foundation (Grant 2014M552229), and the Shenzhen Science and Technology Research Foundation (Grant CXB201005240010A), 111 Program (B08040) of MOE.

DOI: 10.1021/acsami.5b02790
ACS Appl. Mater. Interfaces 2015, 7, 13512–13517

REFERENCES

(1) Zhao, Y.; Hao, X.; Zhang, Q. Energy-Storage Properties and Electrocaloric Effect of $Pb_{1-3x/2}La_xZr_{0.85}Ti_{0.15}O_3$ Antiferroelectric Thick Films. *ACS Appl. Mater. Interfaces* **2014**, *6*, 11633−11639.

(2) Hao, X.; Zhai, J.; Kong, L. B.; Xu, Z. A comprehensive review on the progress of lead zirconate-based antiferroelectric materials. *Prog. Mater. Sci.* **2014**, *63*, 1−57.

(3) Chu, B. J.; Zhou, X.; Ren, K. L.; Neese, B.; Lin, M. R.; Wang, Q.; Bauer, F.; Zhang, Q. M. A dielectric polymer with high electric energy density and fast discharge speed. *Science* **2006**, *313*, 334−336.

(4) Correia, T. M.; McMillen, M.; Rokosz, M. K.; Weaver, P. M.; Gregg, J. M.; Viola, G.; Cain, M. G.; Brennecka, G. L. A Lead-Free and High-Energy Density Ceramic for Energy Storage Applications. *J. Am. Ceram. Soc.* **2013**, *96*, 2699−2702.

(5) Ma, B.; Kwon, D.-K.; Narayanan, M.; Balachandran, U. Dielectric properties and energy storage capability of antiferroelectric $Pb_{0.92}La_{0.08}Zr_{0.95}Ti_{0.05}O_3$ film-on-foil capacitors. *J. Mater. Res.* **2011**, *24*, 2993−2996.

(6) Burn, I.; Smyth, D. M. Energy storage in ceramic dielectrics. *J. Mater. Sci.* **1972**, *7*, 339−343.

(7) Zhang, L.; Jiang, S.; Zeng, Y.; Fu, M.; Han, K.; Li, Q.; Wang, Q.; Zhang, G. Y doping and grain size co-effects on the electrical energy storage performance of $(Pb_{0.87}Ba_{0.1}La_{0.02})(Zr_{0.65}Sn_{0.3}Ti_{0.05})O_3$ antiferroelectric ceramics. *Ceram. Int.* **2014**, *40*, 5455−5460.

(8) Tuttle, B. A.; Payne, D. A. The effects of microstructure on the electrocaloric properties of $Pb(Zr,Sn,Ti)O_3$ ceramics. *Ferroelectrics* **1981**, *37*, 603−606.

(9) Jiang, S.; Zhang, L.; Zhang, G.; Liu, S.; Yi, J.; Xiong, X.; Yu, Y.; He, J.; Zeng, Y. Effect of Zr:Sn ratio in the lead lanthanum zirconate stannate titanate anti-ferroelectric ceramics on energy storage properties. *Ceram. Int.* **2013**, *39*, 5571−5575.

(10) Zhang, G.; Zhu, D.; Zhang, X.; Zhang, L.; Yi, J.; Xie, B.; Zeng, Y.; Li, Q.; Wang, Q.; Jiang, S. High-Energy Storage Performance of $(Pb_{0.87}Ba_{0.1}La_{0.02})(Zr_{0.68}Sn_{0.24}Ti_{0.08})O_3$ Antiferroelectric Ceramics Fabricated by the Hot-Press Sintering Method. *J. Am. Ceram. Soc.* **2015**, *98*, 1175−1181.

(11) Li, X.; Xi, Z.; Long, W.; Fang, P. Synthesis of antiferroelectric $(Bi_{0.534}Na_{0.5})_{0.94}Ba_{0.06}TiO_3$ ceramics with high phase transition temperature and broad temperature range by a solid-state reaction method. *Chin. Sci. Bull.* **2013**, *58*, 2893−2897.

(12) Gao, F.; Dong, X.; Mao, C.; Liu, W.; Zhang, H.; Yang, L.; Cao, F.; Wang, G.; Jones, J. Energy-Storage Properties of $0.89Bi_{0.5}Na_{0.5}TiO_3$−$0.06BaTiO_3$−$0.05K_{0.5}Na_{0.5}NbO_3$ Lead-Free Antiferroelectric Ceramics. *J. Am. Ceram. Soc.* **2011**, *94*, 4382−4386.

(13) Mischenko, A. S.; Zhang, Q.; Scott, J. F.; Whatmore, R. W.; Mathur, N. D. Giant electrocaloric effect in thin-film $PbZr_{0.95}Ti_{0.05}O_3$. *Science* **2006**, *311*, 1270−1.

(14) Ge, J.; Dong, X.; Chen, Y.; Cao, F.; Wang, G. Enhanced polarization switching and energy storage properties of $Pb_{0.97}La_{0.02}(Zr_{0.95}Ti_{0.05})O_3$ antiferroelectric thin films with $LaNiO_3$ oxide top electrodes. *Appl. Phys. Lett.* **2013**, *102*, 142905.

(15) Hao, X.; Zhou, J.; An, S. Effects of PbO Content on the Dielectric Properties and Energy Storage Performance of $(Pb_{0.97}La_{0.02})(Zr_{0.97}Ti_{0.03})O_3$ Antiferroelectric Thin Films. *J. Am. Ceram. Soc.* **2011**, *94*, 1647−1650.

(16) Sa, T.; Qin, N.; Yang, G.; Bao, D. Structure and improved electrical properties of Pr-doped $PbZrO_3$ antiferroelectric thin films with (111) preferential orientation. *Mater. Chem. Phys.* **2013**, *139*, 511−514.

(17) Parui, J.; Krupanidhi, S. B. Enhancement of charge and energy storage in sol−gel derived pure and La-modified $PbZrO_3$ thin films. *Appl. Phys. Lett.* **2008**, *92*, 192901-1−192901-3.

(18) Hao, X.; Zhai, J.; Yao, X. Improved Energy Storage Performance and Fatigue Endurance of Sr-Doped $PbZrO_3$ Antiferroelectric Thin Films. *J. Am. Ceram. Soc.* **2009**, *92*, 1133−1135.

(19) Ye, M.; Sun, Q.; Chen, X.; Jiang, Z.; Wang, F.; Whatmore, R. Effect of Eu Doping on the Electrical Properties and Energy Storage Performance of $PbZrO_3$ Antiferroelectric Thin Films. *J. Am. Ceram. Soc.* **2011**, *94*, 3234−3236.

(20) Li, Q.; Zhang, G.; Liu, F.; Han, K.; Gadinski, M. R.; Xiong, C.; Wang, Q. Solution-processed ferroelectric terpolymer nanocomposites with high breakdown strength and energy density utilizing boron nitride nanosheets. *Energy Environ. Sci.* **2015**, *8*, 922−931.

(21) Parui, J.; Krupanidhi, S. B. Enhancement of charge and energy storage in sol−gel derived pure and La-modified $PbZrO_3$ thin films. *Appl. Phys. Lett.* **2008**, *92*, 192901.

(22) Ge, J.; Remiens, D.; Dong, X.; Chen, Y.; Costecalde, J.; Gao, F.; Cao, F.; Wang, G. Enhancement of energy storage in epitaxial $PbZrO_3$ antiferroelectric films using strain engineering. *Appl. Phys. Lett.* **2014**, *105*, 112908.

(23) Ge, J.; Remiens, D.; Costecalde, J.; Chen, Y.; Dong, X.; Wang, G. Effect of residual stress on energy storage property in $PbZrO_3$ antiferroelectric thin films with different orientations. *Appl. Phys. Lett.* **2013**, *103*, 162903.

(24) Qu, W.; Tan, X. Texture control and ferroelectric properties of $Pb(Nb,Zr,Sn,Ti)O_3$ thin films prepared by chemical solution method. *Thin Solid Films* **2006**, *496*, 383−388.

(25) Pokharel, B. P.; Pandey, D. High temperature x-ray diffraction studies on antiferroelectric and ferroelectric phase transitions in $(Pb_{1-x}Ba_x)ZrO_3$ (x = 0.05,0.10). *J. Appl. Phys.* **2001**, *90*, 2985.

(26) Pandey, S. K.; James, A. R.; Raman, R.; Chatterjee, S. N.; Goyal, A.; Prakash, C.; Goel, T. C. Structural, ferroelectric and optical properties of PZT thin films. *Physica B* **2005**, *369*, 135−142.

(27) Sa, T.; Qin, N.; Yang, G.; Bao, D. W-doping induced antiferroelectric to ferroelectric phase transition in $PbZrO_3$ thin films prepared by chemical solution deposition. *Appl. Phys. Lett.* **2013**, *102*, 172906.

(28) Pasto, A. E.; Condrate, R. A. Raman Spectrum of $PbZrO_3$. *J. Am. Ceram. Soc.* **1973**, *56*, 436−438.

(29) Ke, S.; Fan, H.; Huang, H.; Chan, H. L. W. Lorentz-type relationship of the temperature dependent dielectric permittivity in ferroelectrics with diffuse phase transition. *Appl. Phys. Lett.* **2008**, *93*, 112906.

(30) Peng, B.; Fan, H.; Zhang, Q.; Tan, X. The Contribution of the "Extrinsic" Polarizations to the Dielectric Tunability of $Pb(Mg_{1/3}Nb_{2/3})_{1-x}Ti_xO_3$ Relaxor Ferroelectrics. *J. Am. Ceram. Soc.* **2012**, *95*, 1651−1655.

(31) Zhang, Q. M.; Bharti, V.; Zhao, X. Giant Electrostriction and Relaxor Ferroelectric Behavior in Electron-Irradiated Poly(vinylidene fluoride−trifluoroethylene) Copolymer. *Science* **1998**, *280*, 2101−2104.

(32) Zhang, L.; Hao, X. Dielectric properties and energy-storage performances of $(1-x)(Na_{0.5}Bi_{0.5})TiO_3$−$xSrTiO_3$ thick films prepared by screen printing technique. *J. Alloys Compd.* **2014**, *586*, 674−678.

(33) Zhao, Y.; Hao, X.; Li, M. Dielectric properties and energy-storage performance of $(Na_{0.5}Bi_{0.5})TiO_3$ thick films. *J. Alloys Compd.* **2014**, *601*, 112−115.

DOI: 10.1021/acsami.5b02790
ACS Appl. Mater. Interfaces 2015, 7, 13512−13517